A Potent Aldose Reductase Inhibitor, (2*S*,4*S*)-6-Fluoro-2′,5′-dioxospiro[chroman-4,4′-imidazolidine]-2-carboxamide (Fidarestat): Its Absolute Configuration and Interactions with the Aldose Reductase by X-ray Crystallography

Mitsuru Oka,*,† Yukiharu Matsumoto,‡ Shigeru Sugiyama,§ Nobuaki Tsuruta,‡ and Masaaki Matsushima†,#

Rational Drug Design Laboratories, 4-1-1, Misato, Matsukawa-machi, Fukushima 960-1242, Japan, Sanwa Kagaku Kenkyusyo Company, Ltd., 363, Shiosaki, Hokusei-cho, Inabe-gun, Mie 511-0406, Japan, and Maruwa Food Industry Company, Ltd., 170, Tsutsuji-cho, Yamatokoriyama, Nara 639-1123, Japan

Received October 4, 1999

The absolute configuration of the aldose reductase (AR) inhibitor, (+)-(2*S*,4*S*)-6-fluoro-2′,5′-dioxospiro[chroman-4,4′-imidazolidine]-2-carboxamide (fidarestat), was established indirectly by single-crystal X-ray analysis of (+)-(2*S*,4*S*)-8-bromo-6-fluoro-2′,5′-dioxospiro[chroman-4,4′-imidazolidine]-2-carboxylic acid (**1**). The crystal structure of human AR complexed with fidarestat was determined, and the specific inhibition activity was discussed on the basis of the three-dimensional interactions between them. The structure clarified that fidarestat was located in the active site by hydrophilic and hydrophobic interactions and that the carbamoyl group of fidarestat was a very effective substituent for affinity to AR and for selectivity between AR and aldehyde reductase (AHR). Explanations for the differences between the observed activities of fidarestat and its stereoisomer **2** were suggested by computer modeling.

Introduction

It has been proposed that hyperactivity of the polyol metabolic pathway in individuals with high blood glucose levels induces or contributes to the progression of diabetic complications, i.e., principally neuropathy, retinopathy, and nephropathy.[1] Aldose reductase (AR, EC 1.1.1.21) contributes to the first step of the pathway and catalyzes the reduction of glucose to sorbitol using NADPH as a coenzyme. Therefore, inhibitors of AR have received attention as possible therapeutic drugs for treatment of diabetic complications.

Recently developed potent AR inhibitors can be structurally classified into two main groups, the spirohydantoins, which include sorbinil[2] and fidarestat[3] (Chart 1), and the acetic acid compounds, such as zopolrestat,[4] tolrestat,[5] alrestatin,[6] epalrestat,[7] and zenarestat.[8] In 1992, the X-ray structures of human AR[9,10] and of pig AR[11] were solved. In 1994, a reduction mechanism with NADPH was proposed based on the complexed structures.[12] Further, the structures of complexes with zopolrestat, sorbinil, tolrestat, and alrestatin have been respectively determined to clarify interactions with and the specificities against AR.[13−15]

Fidarestat, which has a spirohydantoin ring and a carbamoyl group, shows a higher activity and a higher selectivity than sorbinil.[3a] In the present study, to relate the biological results to the interactions of fidarestat with AR and to apply these findings to the structure-based drug design of more effective inhibitors, the absolute configuration of fidarestat and the complex structure of AR with fidarestat were determined crystallographically. In addition, the difference in biological activity between fidarestat and its stereoisomer **2** (Chart 1) was also investigated using computer modeling.

Chart 1

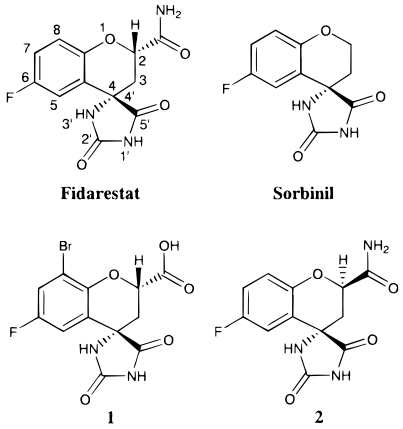

Results and Discussion

Absolute Configuration of Fidarestat. The absolute configuration of fidarestat itself could not be determined because of the insignificant anomalous dispersion effects in the X-ray diffraction intensity observations. Therefore, compound **1** having a bromine atom at the 8-position was prepared from **3** by bromination without racemization, as shown in Scheme 1. The structure of **1** was solved and refined to convergence by single-crystal X-ray analysis. The weighted *R* factor of one of the enantiomers was 5.6%. The signs of the coordinates were reversed, and the other enantiomer

* Author for correspondence. Present address: Sanwa Kagaku Kenkyusyo Co., Ltd., 363, Shiosaki, Hokusei-cho, Inabe-gun, Mie 511-0406, Japan. Tel: 81 594 72 6221. Fax: 81 594 82 0072. E-mail: m_oka@mb6.skk-net.com.
† Rational Drug Design Laboratories.
‡ Sanwa Kagaku Kenkyusyo Co., Ltd.
§ Maruwa Food Industry Co., Ltd.
# Present address: Yamanouchi Pharmaceutical Co., Ltd., 21, Miyukigaoka, Tsukuba-shi, Ibaraki 305-8585, Japan.

10.1021/jm990502r CCC: $19.00
Published on Web 05/18/2000

Scheme 1[a]

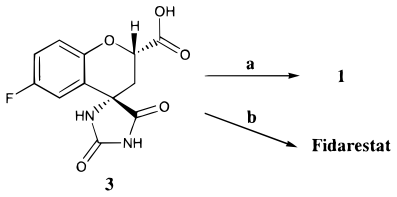

[a] Reagents: (a) Br_2, AcOH; (b)[3b] (i) *n*-PrOH, H_2SO_4, (ii) NH_3/MeOH.

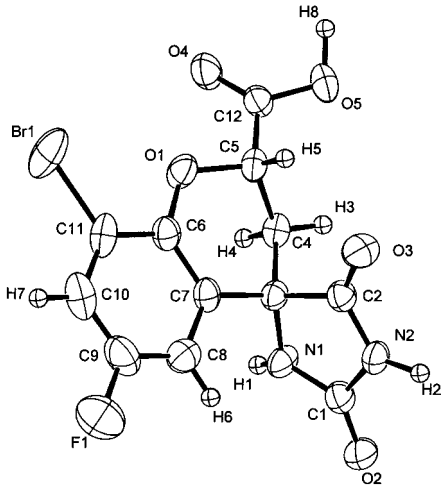

Figure 1. X-ray crystallographic structure of **1**.

was refined to convergence. The weighted *R* factor of the latter enantiomer was 6.4%. The initial enantiomer (2*S*,4*S*) was accepted as the correct enantiomer as rendered in Figure 1. Accordingly, it was indirectly established that the absolute configuration of fidarestat was (2*S*,4*S*), which was identical to the absolute configuration of **1**, since fidarestat was synthesized from the common precursor **3** by the reaction without racemization.[3b]

Complexed Structure of AR with Fidarestat. The X-ray crystal structure of human AR complexed with fidarestat was solved at 2.8 Å resolution by a molecular replacement method using the AR structure in the Brookhaven Protein Data Bank (PDB, accession code 1ADS[9]) as an initial model. The final linear *R* factor of the structure composed of α/β TIM barrels was 19.1%. The $F_{obs} - F_{calc}$ electron density map after the refinements showed clearly the location of fidarestat (Figure 2). Although fidarestat shows a mixed type of noncompetitive and uncompetitive inhibition,[3a] its crystal structure showed that it binded to the active site of the enzyme. The chroman ring was surrounded by the side chains of Trp20, Trp111, Phe122, and Trp219 by hydrophobic interactions. In addition to these, two carbonyl groups in the spirohydantoin ring formed hydrogen bonds with the enzyme by hydrophilic interactions, in a manner similar to that of the carboxyl groups of zopolrestat, torlestat, and alrestatin. One carbonyl group on the 2′-position formed one of the hydrogen bonds with the Oη of Tyr48 (2.6 Å) and was close to the nicotinamide ring of the coenzyme, with the distance to the 4-position carbon of the ring being 2.7 Å. The other carbonyl group on the 5′-postition formed another hydrogen bond with the Nϵ1 of Trp111 (2.7 Å). The distance between the 1′-position nitrogen atom in the hydantoin ring and Nϵ2 of His110 was also suitable for a hydrogen bond (2.8 Å). Further, the structure clarified the role of the carbamoyl group in fidarestat. The oxygen atom of this group was able to form a hydrogen bond with the main-chain nitrogen atom of Leu300 (2.9 Å). Such hydrogen bonds between inhibitors and the nitrogen atom of Leu300 have also been observed in the complexed structures with zopolrestat and alrestatin.[13,14] In sorbinil, the 1-position oxygen atom of the chroman ring forms hydrogen bonds with the main-chain nitrogen atoms of Ala299 and Leu300; however, these are indirect hydrogen bonds made through the water molecules.[15] Sorbinil has no direct hydrogen bonds with any main-chain atoms. It was indicated that the carbamoyl group of fidarestat caused fidarestat to have a higher affinity for AR than sorbinil, as shown in Table 1. The IC_{50} values against human AR are 9 nM for fidarestat and 2000 nM for sorbinil. The fact that fidarestat has a higher affinity than sorbinil against rat AR (the IC_{50} values are 35 nM for fidarestat and 900 nM for sorbinil (Table 1)) might also be explained by

Table 1. In Vitro IC_{50} Values (nM) of Inhibitors Against AR and AHR

compd	rat AR	human AR	human AHR
fidarestat	35[a]	9[b]	1200[b]
sorbinil	900[a]	2000[c]	5400[c]
2	570[a]		

[a] Data from Yamaguchi et al.[3b] [b] Data from Mizuno et al.[3a] [c] Data from Barski et al.[22]

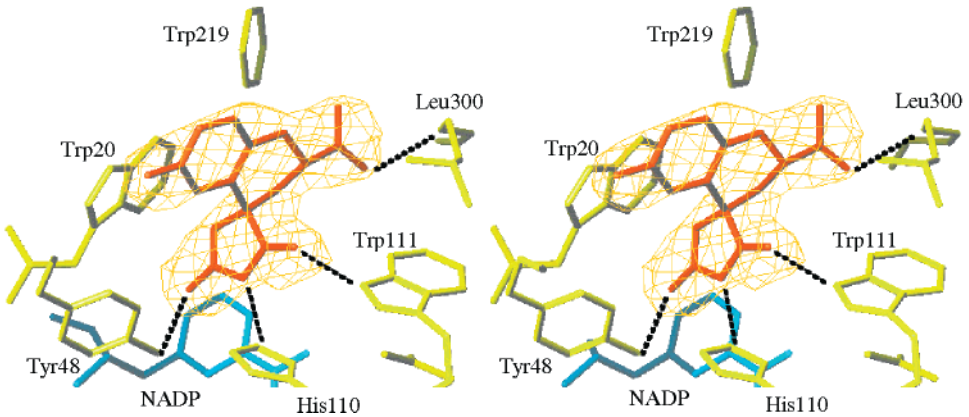

Figure 2. Stereoscopic $F_{obs} - F_{calc}$ electron density map around fidarestat (red) after the refinements. All of the fidarestat contributions were deleted from the map calculations. The hydrogen bonds are represented by dotted lines.

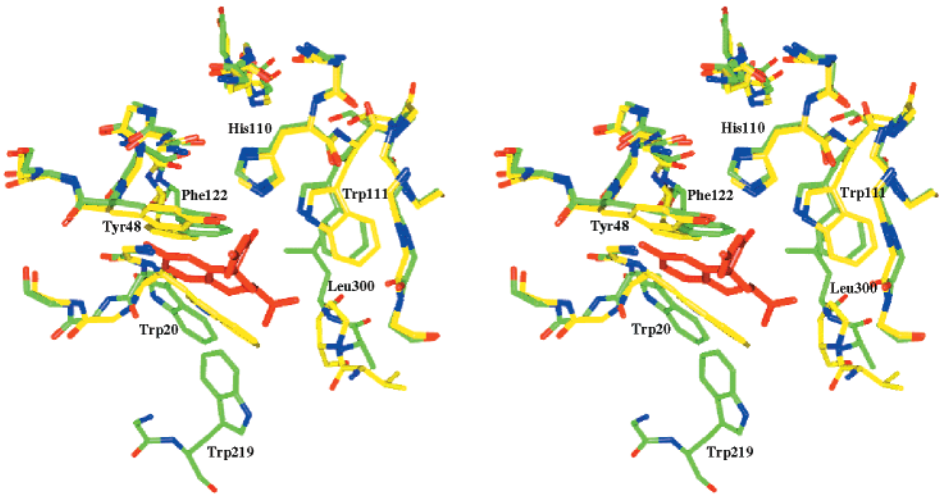

Figure 3. Superimposition of AHR[16] (yellow) on AR (green) with fidarestat (red). Onto the main-chain atoms of Trp20, Tyr48, His110, Trp111, and Phe122 in AR were superimposed the corresponding residues in AHR. Trp219 in AR was not used, because of the absence of the atomic coordinates of the corresponding residues in AHR. The residue of Leu300 in AR was exchanged for proline in AHR. The residue numbers of AR were used. NADP was not included in this figure.

the presence of the hydrogen bond, because Leu300 is conserved between human AR and rat AR.[16]

Selectivity of Fidarestat between AR and AHR. One of the important factors in preventing possible side effects of inhibitors is their selectivity against similarly functioning proteins. AR and aldehyde reductase (AHR) are members of the aldo-keto reductase superfamily and reduce aldehyde compounds using NADPH as a coenzyme. Human AR has 65% sequence homology to human AHR.[17] The six residues described in the previous section, Trp20, Tyr48, His110, Trp111, Phe122, and Trp219, are conserved in human AHR, based on the sequence comparison.[17] Three-dimensional structuralization of human and porcine AHR has shown that both are composed of α/β TIM barrels and both have structures similar to that of AR.[18,19] And structuralization of the complex formed by AHR and tolrestat has shown that the six conserved residues are located in the binding site of the inhibitor.[20]

Our superimposition of human AHR (PDB accession code 2ALR[18]) onto human AR with fidarestat also indicated that these conserved residues in AHR were located in close proximity to those in AR, as shown in Figure 3. This fact suggested that fidarestat would bind to AHR in the same manner as to AR. However, Leu300 in AR, which interacts with fidarestat by one of the hydrogen bonds, is not conserved in AHR.[17] As shown in Figure 3, Leu300 in AR corresponded to the proline residue in AHR. This substitution of Leu300 in AR to proline in AHR might be one of the major factors for the 133-fold activity reduction, because the proline residue in AHR could not form a hydrogen bond with fidarestat (the IC_{50} values of fidarestat are 9 nM against human AR and 1200 nM against human AHR, as shown in Table 1).

A previous study[21] on the complex structures of AR with zopolrestat[13] and AHR with tolrestat[19] has shown that the 450-fold differences in the potency of inhibition of AHR and AR by zopolrestat are reflected in the mode of the interactions of the inhibitor with the enzymes. In their discussion, other authors pointed out that one of the differences of the binding site between AR and AHR is the substitution of Leu300 in AR to a proline residue in AHR.[20,21] That is, zoplrestat has one hydrogen bond with the main-chain nitrogen atom of Leu300.[13]

On the other hand, sorbinil may have no selectivity because it has no substituent on the 2-position with which to form hydrogen bonds (the IC_{50} values of sorbinil are 2000 nM against AR and 5400 nM against AHR, as shown in Table 1). These conjectures could be resolved by further X-ray studies.

Modeled Structure of the Stereoisomer. The affinity of stereoisomer **2** to AR is lower than that of fidarestat to AR, as shown in Table 1 (the IC_{50} values against rat AR are 570 nM for **2** and 35 nM for fidarestat). On the supposition that the binding mode of the isomer was similar to that of fidarestat, the complexed structure of **2** with AR was modeled based on the X-ray structure, as shown in Figure 4 (see Experimental Section). The complexed structure showed that the hydrogen bond length between the oxygen atom of the carbamoyl group in **2** and the nitrogen atom of LEU300 was longer than that in the complex structure with fidarestat (the former was 3.2 Å, the latter 2.9 Å) and also showed the subtle difference in direction of the hydantoin rings between them. These observations might explain the difference of the affinities between **2** and fidarestat against AR. It was suggested that the isomer **2** might bind to AR in a manner similar to the binding of fidarestat to AR and that the stereochemistry of the carbamoyl group might have marked influences on the affinity to AR.

Conclusion

The crystal structure of AR complexed with fidarestat clearly demonstrated the interactions between AR and fidarestat. We noted that the carbamoyl group formed a hydrogen bond with the main-chain nitrogen atom of Leu300. It was suggested that the interaction caused a higher affinity of fidarestat to AR than that of sorbinil, which has no substituent at the 2-position, to AR. Furthermore, it was demonstrated that the substituent enhanced the selectivity between AR and AHR and that the active-site configuration of the substituent was more favorable to the affinity to AR than to the affinity to

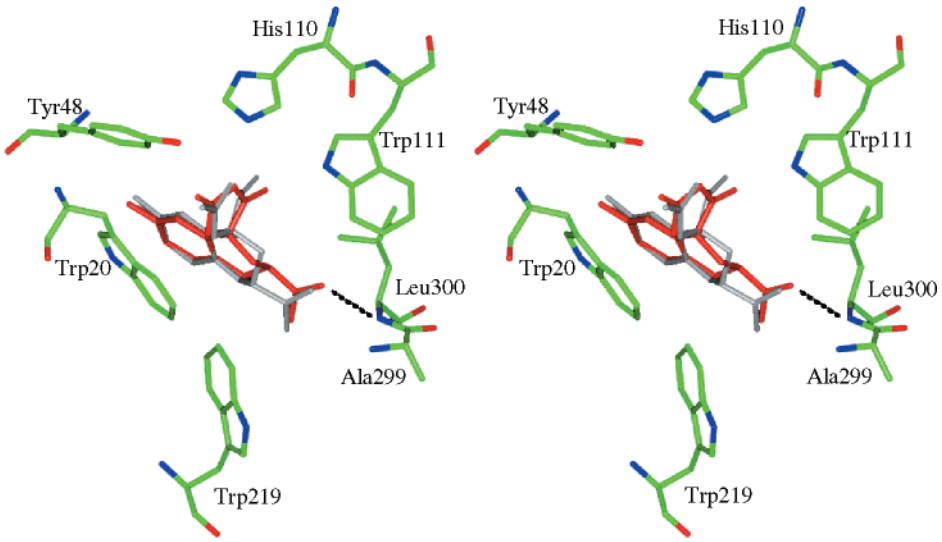

Figure 4. Superimposition of fidarestat (red) in the complex structure by X-ray structure analysis and its stereoisomer **2** (gray) by computer modeling. These inhibitors and the surrounding seven residues are shown. The hydrogen bond to the carbamoyl group with AR is represented by a dotted line.

AR of its stereoisomer. These results indicate that additional analysis of the derivatives of fidarestat might lead to the design of more effective AR inhibitors.

Experimental Section

Melting points were measured on a Yanaco MP-1 apparatus and were uncorrected. Optical rotations were obtained on a Jasco DIP-360 polarimeter. Infrared (IR) spectra were recorded on a Jasco IR-810 spectrophotometer. NMR spectra were recorded on a JEOL JNM-GSX270 spectrometer (270 MHz for ^{1}H and 68 MHz for ^{13}C) in $CDCl_3$ with tetramethysilane as an internal standard. Mass spectra were obtained on a JEOL JMS-DX300 or JMS-SX102A. All reagents were purchased at highest commercial quality and used without further purification. Compound **1** was prepared according to known procedures.[3b]

(+)-(2*S*,4*S*)-8-Bromo-6-fluoro-2′,5′-dioxospiro[chroman-4,4′-imidazolidine]-2-carboxylic Acid (1). To a solution of **3** (2.80 g, 10.0 mmol) in acetic acid (20 mL) was added dropwise bromine (7.99 g, 50.0 mmol) at 100 °C, and the mixture was stirred at 100 °C for 24 h. The resulting precipitate was recrystallized from 100 mL of 0.1 M HCl to give **1** (2.60 g, yield 73.0%) as colorless prisms: mp 263−264 °C; $[\alpha]^{29}_{D}$ +142.0° (c = 1.0, MeOH); IR (KBr, cm^{-1}) 3400 (COOH), 1775 and 1725 (C=O of hydantoin); ^{1}H NMR (DMSO-d_6) δ 2.17 (1H, dd, J = 13.7, 12.2 Hz, H3α), 2.60 (1H, dd, J = 13.7, 2.4 Hz, H3β), 5.24 (1H, dd, J = 12.2, 2.4 Hz, H2), 7.08 (1H, dd, J = 8.8, 2.9 Hz, H5), 7.59 (1H, dd, J = 7.8, 2.9 Hz), 8.36 (1H, brs, *H*-N3′), 11.05 (1H, brs, *H*-N1′); ^{13}C NMR (DMSO-d_6) δ 32.1 (C3), 59.2 (C4), 71.8 (C2), 110.7 (C4a), 111.9 (C5), 120.7 (C7), 122.5 (C8), 147.2 (C8a), 155.6 (C6), 156.1 (C2′), 169.3 (COOH), 175.7 (C5′); LRMS (EI) m/z 358 (M^+); HRMS (EI) calcd for $C_{12}H_8BrFN_2O_5$ (M^+) 357.9601, found 357.9585.

Crystallographic Study of 1. A colorless prismatic crystal (0.10 × 0.25 × 0.25 mm^3) of **1** was grown from water at 20−25 °C and measured on a Rigaku AFC5R diffractometer with graphite monochromated Cu Kα radiation (λ = 1.5418 Å) and a 12-kW rotating anode generator. The unit cell was determined from the setting angles of 25 carefully centered reflections in the range 78.20° < 2θ < 79.73°. The space group was determined from the systematic absences. The data were collected at a temperature of 23 ± 1 °C using the ω−2θ scan technique to a maximum 2θ value of 124.1°. Scans of (1.31 + 0.30 tan θ)° were made at a speed of 32.0°/min (in ω). Stationary background counts were recorded on each side of the reflection. For all calculations, the teXsan crystallographic software package (Molecular Structure Corp.) was used. The structure was solved by a direct method. The non-hydrogen atoms were refined anisotropically. Hydrogen atoms were included in the structure factor calculation in idealized positions (dC−H = 0.95 Å).

Crystal data of 1: $C_{12}H_{14}BrFO_8N_2$, M = 413.15, orthorhombic, $P2_12_12_1$, a = 11.792(1) Å, b = 15.742(2) Å, c = 8.729(1) Å, V = 1620.4(3) Å^3, Z = 4, D_{calc} = 1.693 g/cm^3, F(000) = 832, μ(Cu Kα) = 39.94 cm^{-1}; 1501 reflections were measured, refinement = 1370 reflections ($I > 3.00\,\sigma(I)$) and 227 variables, R = 0.036 and R_w = 0.051.

Crystallographic Study of the AR−Fidarestat Complex. Human AR (Wako Pure Chemical Industries) was used without further purification. The crystals of the complex were grown from small crystals at 4 °C in the presence of 2-fold molar fidarestat by a hanging drop vapor diffusion method. The reservoir solution contained 1.8 M ammonium sulfate, 2% PEG400 and 0.1 M HEPES−NaOH (pH 7.5). X-ray intensity data were collected at 8 °C using a diffractometer equipped with an Imaging Plate (DIP-2000; MAC-Science) on a rotating anode X-ray generator operated at 50 mA and 90 kV with a bent double-mirror system (M18X; MAC-Science). The evaluation of the measured intensities was performed by the program DENZO.[23] The collected 27 091 observed reflections from four crystals were merged by the program PROTEIN[24] to give 15 960 unique reflections with 92.4% completeness and 7.05% R_{merge} at 2.8 Å resolution. The crystals belonged to space group C2 with the cell constants of a = 96.14 Å, b = 62.56 Å, c = 118.99 Å and β = 101.6 Å. It was estimated that two protein molecules were in an asymmetric unit. The complexed structure was solved by a molecular replacement method in the XPLOR program suite[25] using the AR structure (PDB accession code 1ADS) as a model structure. The refinements for 8.0−2.8 Å resolution were performed with XPLOR and interactive manual corrections with TURBO-FRODO[26] to obtain the final structure in 19.1% of R factor (27.8% of free R factor). rms deviations were 0.014 Å for bond length, 1.681° for bond angles, 23.2° for torsion angles and 1.560° for improper angles. Only overall isotropic B factor was refined to 4.96 Å^2. The atomic parameters were refined without the individual B factors, since the number of parameters, 15 561, included in the refinements was greater than the number of structure factors, 14 920. The mean error in the refined coordinates was estimated to be 0.21 Å.[27] The coordinates have been deposited at the Brookhaven Protein Data Bank under the PDB ID code 1EF3.

Molecular Modeling. The stereoisomer **2** was modeled based on the coordinate of **1**. Considering that the carboxyl group of **1** was in the equatorial orientation in the half-chair form and that the 1,3-diaxial interaction occurred in the case

of the axial orientation, it was thought appropriate to position the carbamoyl group of the isomer **2** in an equatorial orientation. Therefore, after conversion of the carboxyl group to a carbamoyl group and removal of the bromine atom in **1**, the half-chair form was flipped and then minimized. The resulting structure **2** was inserted into the active site of AR by superimposing the heteroatoms of the chroman ring and hydantoin ring of **2** onto the heteroatoms of the corresponding rings of fidarestat. The carbamoyl group of **2** was minimized in fixing the coordinates of other atoms. All molecular modeling was performed using the software package QUANTA/CHARMm.[28]

Acknowledgment. We thank Dr. T. Ikami for his assistance with the mass spectral measurements.

References

(1) Kinoshita, J. H.; Nishimura, C. The Involvement of Aldose Reductase in Diabetic Complications. *Diabetes Metab. Rev.* **1988**, *4*, 323−337.

(2) Sarges, R.; Bordner, J.; Dominy, B. W.; Peterson, M. J.; Whipple, E. B. Synthesis, Absolute Configuration, and Conformation of the Aldose Reductase Inhibitor Sorbinil. *J. Med. Chem.* **1985**, *28*, 1716−1720.

(3) (a) Mizuno, K.; Yamaguchi, T.; Inoue, A.; Tomiya, N.; Unno, R.; Miura, K.; Usui, T.; Matsumoto, Y.; Kondo, Y.; Yoshina, S.; Kondo, Y.; Sato, M.; Matsubara, A.; Kato, N.; Nakano, K.; Shirai, M.; Inoue, T.; Awaya, J.; Asaeda, N.; Hayasaka, I.; Koide, M.; Hibi, C.; Ban, M.; Sawai, K.; Kurono, M. Profile of a new aldose reductase inhibitor, (*2S*,*4S*)-6-fluoro-2′,5′-dioxospiro[chroman-4,4′-imidazolidine]-2-carboxamide. *Excerpta Med.* **1990**, *913*, 89−96. (b) Yamaguchi, T.; Miura, K.; Usui, T.; Unno, R.; Matsumoto, Y.; Fukushima, M.; Mizuno, K.; Kondo, Y.; Baba, Y.; Kurono, M. Synthesis and Aldose Reductase Inhibitory Activity of 2-Substituted-6-Fluoro-2,3-dihydrospiro[4H-1-benzopyran-4,4′-imidazolidine]-2′,5′-diones. *Arzneim.-Forsch./Drug Res.* **1994**, *44*, 344−348.

(4) Mylari, B. L.; Larson, E. R.; Beyer, T. A.; Zembrowski, W. J.; Aldinger, C. E.; Dee, M. F.; Siegel, T. W.; Singleton, D. H. Novel, Potent Aldose Reductase Inhibitors: 3,4-Dihydro-4-oxo-3-[[5-(trifluoromethyl)-2-benzothiazolyl]methyl]-1-phthalazineacetic Acid (Zopolrestat) and Congeners. *J. Med. Chem.* **1991**, *34*, 108−122.

(5) Sestanj, K.; Bellini, F.; Fung, S.; Abraham, N.; Treasurywala, A.; Humber, L.; Simard-Duquesne, N.; Dvornik, D. N-[[5-(Trifluoromethyl)-6-methoxy-1-naphthalenyl]thioxomethyl]-*N*-methylglycine (Tolrestat), a Potent, Orally Active Aldose Reductase Inhibitor. *J. Med. Chem.* **1984**, *27*, 255−256.

(6) Dvornik, D.; Simard-Duquesne, N.; Krami, M.; Sestanj, K.; Gabbay, K. H.; Kinoshita, J. H.; Varma, S. D.; Merola, L. O. Polyol Accumulation in Galactosemic and Diabetic Rats: Control by an Aldose Reductase Inhibitor. *Science* **1973**, *182*, 1146−1148.

(7) Kikkawa, R.; Hatanaka, I.; Yasuda, H.; Kobayashi, N.; Shigeta, Y.; Terashima, H.; Morimura, T.; Tsuboshima, M. Effect of A New Aldose Reductase Inhibitor, (E)-3-Carboxymethyl-5-[(2E)-Methyl-3-Phenylpropenylidene]Rhodanine (ONO2235), on Peripheral Nerve Disorders in Streptozotocin-Diabetic Rats. *Diabetologia* **1983**, *24*, 290−292.

(8) Ao, S.; Shingu, Y.; Kikuchi, C.; Takano, Y.; Nomura, K.; Fujiwara, T.; Ohkubo, Y.; Notsu, Y.; Yamaguchi, I. Characterization of a Novel Aldose Reductase Inhibitor, FR74366, and its Effects on Diabetic Cataract and Neuropathy in the Rats. *Metabolism* **1991**, *40*, 77−87.

(9) Wilson, D. K.; Bohren, K. M.; Gabbay, K. H.; Quiocho, F. A. An Unlikely Sugar Substrate Site in the 1.65 Å Structure of the Human Aldose Reductase Holoenzyme Implicated in Diabetic Complications. *Science* **1992**, *257*, 81−84.

(10) Borhani, D. W.; Harter, T. M.; Petrash, J. M. The Crystal Structure of the Aldose Reductase•NADPH Binary Complex. *J. Biol. Chem.* **1992**, *267*, 24841−24847.

(11) Rondeau, J.-M.; Tête-Favier, F.; Podjarny, A.; Reymann, J.-M.; Barth, P.; Biellmann, J.-F.; Moras, D. Novel NADPH-binding domain revealed by the crystal structure of aldose reductase. *Nature* **1992**, *355*, 469−472.

(12) Harrison, D. H.; Bohren, K. M.; Ringe, D.; Petsko, G. A.; Gabbay, K. H. An Anion Binding Site in Human Aldose Reductase: Mechanistic Implications for the Binding of Citrate, Cacodylate, and Glucose 6-Phosphate. *Biochemistry* **1994**, *33*, 2011−2020.

(13) Wilson, D. K.; Tarle, I.; Petrash, J. M.; Quiocho, F. A. Refined 1.8 Å structure of human aldose reductase complexed with the potent inhibitor zopolrestat. *Proc. Natl. Acad. Sci. U.S.A.* **1993**, *90*, 9847−9851.

(14) Harrison, D. H. T.; Bohren, K. M.; Petsko, G. A.; Ringe, D.; Gabbay, K. H. The Alrestatin Double-Decker: Binding of Two Inhibitor Molecules to Human Aldose Reductase Reveals a New Specificity Determinant. *Biochemistry* **1997**, *36*, 16134−16140.

(15) Urzhumtsev, A.; Tête-Favier, F.; Mitschler, A.; Barbanton, J.; Barth, P.; Urzhumtseva, L.; Biellmann, J.-F.; Podjarny, AD.; Moras, D. A 'specificity' pocket inferred from the crystal structures of the complexes of aldose reductase with the pharmaceutically important inhibitors tolrestat and sorbinil. *Structure* **1997**, *5*, 601−612.

(16) Chung, S.; LaMendola, J. Cloning and Sequence Determination of Human Placental Aldose Reductase Gene. *J. Biol. Chem.* **1989**, *264*, 14775−14777.

(17) Bohren, K. M.; Bullock, B.; Wermuth, B.; Gabbay, K. H. The Aldo-Keto Reductase Superfamily. *J. Biol. Chem.* **1989**, *264*, 9547−9551.

(18) El-Kabbani, O.; Green, N. C.; Lin, G.; Carson, M.; Narayana, S. V. L.; Moore, K. M.; Flynn, T. G.; DeLucas, L. J. Structures of Human and Porcine Aldehyde Reductase: an Enzyme Implicated in Diabetic Complications. *Acta Crystallogr.* **1994**, *D50*, 859−868.

(19) El-Kabbani, O.; Judge, K.; Ginell, S. L.; Myles, D. A. A.; DeLucas, L. J.; Flynn, T. G. Structure of porcine aldehyde reductase holoenzyme. *Nature Struct. Biol.* **1995**, *2*, 687−692.

(20) El-Kabbani, O.; Carper, D. A.; McGowan, M. H.; Devedjiev, Y.; Rees-Milton, K. J.; Flynn, T. G. Studies on the Inhibitor-Binding Site of Porcine Aldehyde Reductase: Crystal Structure of the Holoenzyme−Inhibitor Ternary Complex. *Proteins: Struct., Funct., Genet.* **1997**, *29*, 186−192.

(21) El-Kabbani, O.; Wilson, D. K.; Petrash, J. M.; Quiocho, F. A. Structural Features of the Aldose Reductase and Aldehyde Reductase Inhibitor-Binding Sites. *Mol. Vision* **1998**, *4*, 19−25.

(22) Barski, O. A.; Gabbay, K. H.; Grimshaw, C. E.; Bohren, K. M. Mechanism of Human Aldehyde Reductase: Characterization of the Active Site Pocket. *Biochemistry* **1995**, *34*, 11264−11275.

(23) Otwinoski, Z. DENZO; 1993.

(24) Steigemann, W. PROTEIN, revision 5; Max-Planck-Institute for Biochemistry, 1993.

(25) Brünger, A. T. XPLOR, version 3.1. *A System for X-ray Crystallography and NMR*; Yale University Press, 1992.

(26) TURBO-FRODO, version 5.0; Bio-Graphics, March 1994.

(27) Luzzati, P. V. Traitement Statistique des Erreurs dans la Determination des Structures Cristallines. *Acta Crystallogr.* **1952**, *5*, 802−810.

(28) QUANTA/CHARMm was developed by Molecular Simulations Inc.

JM990502R